ACS APPLIED MATERIALS & INTERFACES

Research Article

www.acsami.org

Two-Photon Polymerization of Sub-micrometric Patterned Surfaces: Investigation of Cell-Substrate Interactions and Improved Differentiation of Neuron-like Cells

Attilio Marino,*[,†,‡] Gianni Ciofani,[†] Carlo Filippeschi,[†,‡] Mario Pellegrino,[§] Monica Pellegrini,[∥] Paolo Orsini,[§] Massimo Pasqualetti,[⊥] Virgilio Mattoli,[†] and Barbara Mazzolai[†]

[†]Center for Micro-BioRobotics @SSSA, Istituto Italiano di Tecnologia, Viale Rinaldo Piaggio 34, 56025 Pontedera, Italy

[‡]The Biorobotics Institute, Scuola Superiore Sant'Anna, Viale Rinaldo Piaggio 34, 56025 Pontedera, Italy

[§]Dipartimento di Ricerca Traslazionale e delle Nuove Tecnologie in Medicina e Chirurgia University of Pisa, Via Savi 10, 56126 Pisa, Italy

[∥]Scuola Normale Superiore di Pisa, Piazza dei Cavalieri 7, 56126 Pisa, Italy

[⊥]Dipartimento di Biologia, University of Pisa, Via Luca Ghini 13, 56126 Pisa, Italy

Supporting Information

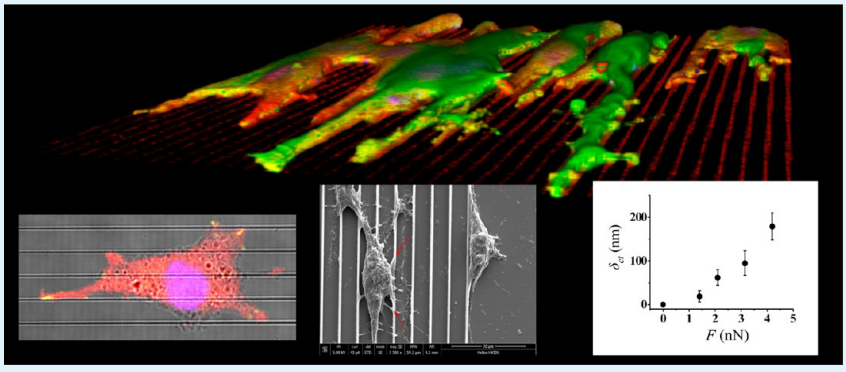

ABSTRACT: Direct Laser Writing (DLW) is an innovative tool that allows the photofabrication of high resolution 3D structures, which can be successfully exploited for the study of the physical interactions between cells and substrates. In this work, we focused our attention on the topographical effects of submicrometric patterned surfaces fabricated *via* DLW on neuronal cell behavior. In particular, we designed, prepared, and characterized substrates based on aligned ridges for the promotion of axonal outgrowth and guidance. We demonstrated that both rat PC12 neuron-like cells and human SH-SY5Y derived neurons differentiate on parallel 2.5 μm spaced submicrometric ridges, being characterized by strongly aligned and significantly longer neurites with respect to those differentiated on flat control substrates, or on more spaced (5 and 10 μm) ridges. Furthermore, we detected an increased molecular differentiation toward neurons of the SH-SY5Y cells when grown on the submicrometric patterned substrates. Finally, we observed that the axons can exert forces able of bending the ridges, and we indirectly estimated the order of magnitude of these forces thanks to scanning probe techniques. Collectively, we showed as submicrometric structures fabricated by DLW can be used as a useful tool for the study of the axon mechanobiology.

KEYWORDS: *Direct Laser Writing, bio/nonbio interfaces, neuronal tissue engineering, nerve regeneration, axonal guidance, biomechanics*

1. INTRODUCTION

Direct Laser Writing (DLW) is a versatile photolithographic technique that takes advantage of the two-photon polymerization (2pp) of dedicated resists for the fabrication of high-resolution 2D and 3D structures.[1−3] Furthermore, DLW allows for a more rapid prototyping of these structures when compared to more traditional lithography techniques, which instead require several processing steps.[4]

A number of studies demonstrated as DLW is a promising tool for the preparation of nanostructured scaffolds suitable for cell culturing.[5−7] In particular, substrates obtained by DLW were used to control the cell behavior as well as to measure the forces that cells exert on the substrate itself.[8−10]

The ideal material for the preparation of substrates used for the investigation of these phenomena should be biocompatible and should allow the photofabrication of flexible structures with

Received: September 9, 2013
Accepted: December 5, 2013
Published: December 5, 2013

high reproducibility. Ormocomp (commercially available from Micro Resist Technology) is a well characterized biocompatible hybrid polymer,[11] exploited for the fabrication of biomedical microdevices[12,13] and for the preparation of scaffolds in tissue engineering.[14,15] Ormocomp patterned substrates have been widely used for the *in vitro* investigation of cell behaviors. As an example, 2pp of Ormocomp scaffolds characterized by ridges of different heights was used for the investigation of fibroblast contact guidance.[4] In another work, Ormocomp micropatterns of different widths and divergence angles were used to quantitatively investigate fibroblast migration.[16] It has also been demonstrated the possibility to photofabricate Ormocomp elastic scaffolds suitable for the measurement of the cardiomyocyte contraction forces during beating:[10] thanks to this approach, it was possible to infer the magnitude of very small forces, of a few nN.

In tissue engineering, the exploitation of an appropriate material for the scaffold fabrication is of paramount importance but even the substrate topography is crucial for the proper cell−substrate interaction.[17,18] The control of the surface geometry is essential for the cellular proliferation, migration, and differentiation toward a specific lineage and eventually for particular cell morphology and function maturation.[19−26] In particular, the investigation of the microenvironment effects on the neural differentiation is a particularly interesting topic not only for tissue engineering but also for regenerative medicine.[27]

Concerning neural tissue engineering, the promotion of the axonal outgrowth and its guidance toward appropriate targets are intensively investigated,[28−32] since these phenomena play a key role for the generation of the correct architecture of the neural network, and are fundamental for the design of efficient artificial nerve conduits,[33,34] as well as for biohybrid neuronal interfaces manufacturing.[35] During the nervous system development, several physical and chemical cues direct the neurite outgrowth.[36−38] In particular, in the axonal fasciculation, growing fibers adhere to pioneer axons and follow their direction.[39] Several studies pretended to reproduce these stimuli *in vitro* in order to control the axonal path-finding and to promote the correct neural morphogenesis.[40,41] Concerning mechanical cues, different surface features such as pillars, grooves, and ridges are able to promote and direct the axonal elongation *in vitro*.[42−44] It has been demonstrated that axons can interact with surface features of a few hundreds of nanometers,[45] but more pronounced effects on neurite formation, alignment, and length were obtained when grooves and ridges have sizes comparable to those of the axons.[46,47]

As previously mentioned, substrates can mechanically stimulate the cells but, *vice versa*, cells are conversely able to exert forces and deform elastic structures. It is possible to infer the magnitude of these forces by knowing the mechanical properties of the structures, for example, by deforming them with calibrated forces through atomic force microscopy (AFM). Moreover, since the level of the structure deformations directly depends on the force intensity applied by the cells, it is also possible to deduce these forces optically, by measuring the substrate deformation. In this way, micro- or nanotopography arrays have became a high-throughput and cost-effective tool for the study of cell mechanobiology.[48−50]

In this paper, we propose the DLW technique for the rapid prototyping of submicrometric structures dedicated to the study of neuron-substrate interactions. In particular, the aim of this work is to photofabricate ridges that mimic the physical presence of other axons and to test the effects of these topographical cues on the axonal guidance and on the promotion and improvement of neurite outgrowth. Furthermore, we investigated the effects of the topography cues on the molecular differentiation of the considered cell lines. Finally, we were able to measure the deformations of the ridges induced by the neural branches and thus, thanks to scanning probe techniques, to indirectly estimate the intensity of the forces applied by the cells to the substrates.

2. EXPERIMENTAL SECTION

2.1. Substrate Preparation and Characterization. Submicrometric patterned surfaces were fabricated by a commercially available two photon DLW system (Photonic Professional, Nanoscribe GmbH) equipped with an inverted microscope (Zeiss) and a 100× immersion objective, numerical aperture = 1.4. Two photons of 790 nm, pulsed at 120 fs, were used to cure a biocompatible UV-curable photoresists (Ormocomp) on glass coverslips. Single ridges were polymerized on the glass surface using a laser power of 10 mW and a scan speed of 50 μm/s. Aligned ridges at a distance of 10 μm, 5 μm, or 2.5 μm were thus written (in the following and in the figures respectively named as substrates 2, 3, and 4; flat control substrate will be indicated as substrate 1). The unexposed region of the resist was dissolved by washing the glass coverslips with the Ormodev (Micro Resist Technology) developer. Finally, coverlips were washed with isopropyl alcohol and subsequently with deionized water.

Obtained substrates were characterized by scanning electron microscopy (SEM) and atomic force microscopy (AFM). For SEM imaging, the substrates were gold-sputtered for 25 s at 60 nA. Imaging was performed by using a EVO MA10 (Zeiss). A focused ion beam (FIB) system (FEI Helios 600) was used to mill the ridge, by using an accelerating voltage of 30 kV and a milling current of 2 pA.

The AFM acquisitions were carried out with a diINNOVA SPM system (Bruker) in tapping mode, equipped with a cantilever owning a tip radius of 8 nm and a full tip cone angle of 40°. The cantilever elastic constant and the resonance frequency were 46 N/m and 325 kHz, respectively. For the roughness evaluation, a cantilever equipped with a tip radius of 6 nm was adopted, characterized by an elastic constant of 5.1 N/m of and by a resonance frequency of 150 kHz.

2.2. Cell Cultures. Two different *in vitro* neuronal models were investigated. The PC12 cell line (ATCC CRL-1721) derived from rat adrenal pheochromocytoma was adopted because of its capability to reversibly respond to Nerve Growth Factor (NGF) stimulation, expressing specific neural marker and extending neurites similar to those of sympathetic neurons.[51] PC12 neuron-like cells were plated on collagen-coated T-75 flasks and cultured in Dulbecco's modified Eagle medium (DMEM) supplemented with 5% fetal bovine serum (FBS), 10% horse serum (HS), 2 mM L-glutamine, 100 U/ml penicillin, and 100 μg/mL streptomycin. The medium was changed every two days and undifferentiated cells were split 1:3 every 5 days using trypsin at a concentration of 0.05% with 0.02% EDTA. For the differentiation experiments, PC12 cells were plated at a density of 15,000 cell/cm^2 on the collagen-coated substrates and maintained for 5 days in DMEM supplemented with 1% FBS, 100 ng/mL NGF, 100 U/ml penicillin, and 100 μg/mL streptomycin. Differentiation medium was replaced every 2 days.

SH-SY5Y human neuroblastoma derived cell line (ATCC CRL-2266) was adopted as *in vitro* model of differentiation toward neurons characterized by adrenergic and cholinergic phenotypes.[52] SH-SY5Y cells were cultured in T-75 flask in DMEM/F12 with 10% FBS, 100 U/ml penicillin, and 100 μg/mL streptomycin, and then differentiated at a density of 20 000 cell/cm^2 on the collagen-coated substrates for 5 days in DMEM with 1% FBS, 10 μM all-trans-retinoic acid (RA), 100 U/ml penicillin, and 100 μg/mL streptomycin.

2.3. Biological Testing. After 5 days since differentiation induction, samples were washed with PBS and then fixed with 4% paraformaldehyde in PBS at 4 °C for 20 min.

The immunostaining of β3-tubulin was performed following standard immunocytochemistry procedures, with an incubation of samples in a 1:75 diluted solution of a rabbit IgG primary antibody in

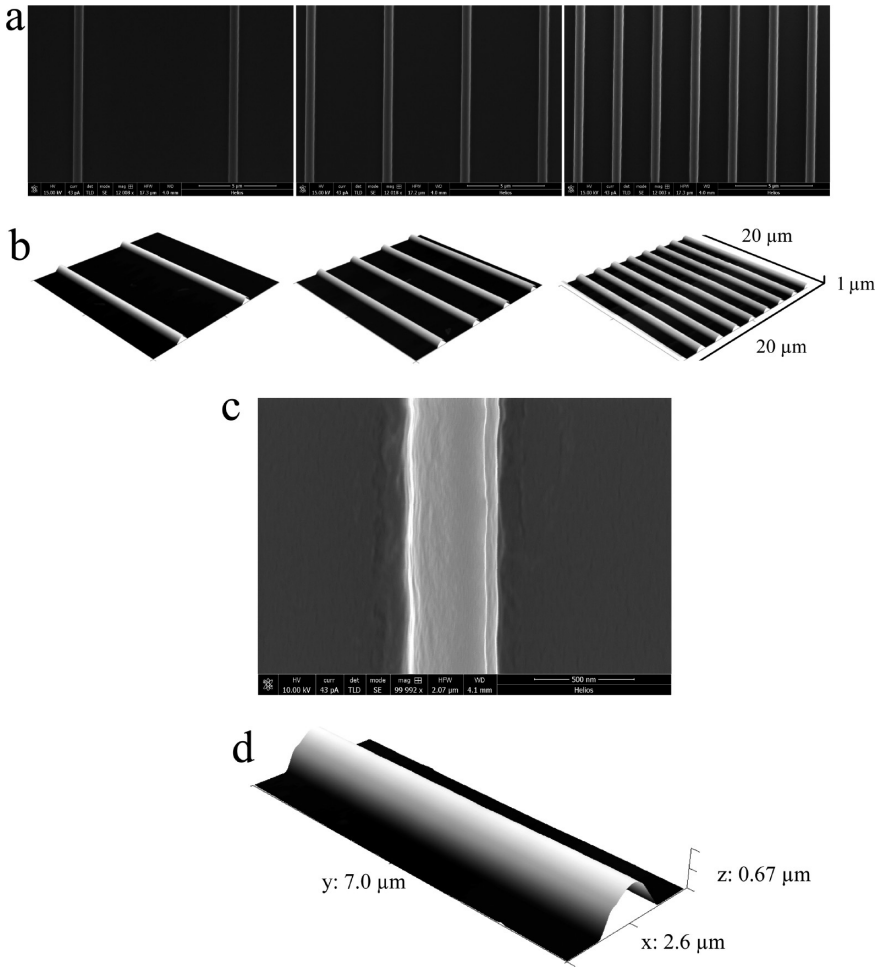

Figure 1. Characterization of the substrates fabricated by the two photon polymerization of Ormocomp. (a) SEM acquisitions showing patterned surfaces characterized by low, intermediate, and high frequency of submicrometric ridges. (b) AFM images of the substrates. (c and d) SEM and AFM high magnifications of a single ridge.

10% goat serum (Sigma), followed by an incubation with a 1:250 diluted solution of goat Alexa Fluor 488-IgG antirabbit secondary antibody (Invitrogen). The immunostaining of vinculin was performed with a 1:50 dilution of the primary mouse IgG antibody (Millipore) followed by treatment with a 1:50 dilution of the secondary goat FITC-IgG antimouse (Millipore). Cytoskeletal f-actin and cell nucleus staining were obtained using respectively TRITC-conjugated phalloidin (Sigma) and DAPI (Millipore), according to the manufacturers' protocols. Fluorescence images were acquired with both epifluorescence (Eclipse Ti, Nikon) and confocal microscope (C2s, Nikon). NIS professional software was used for the 3D reconstruction of *z*-stacks collected by confocal microscopy.

For the SEM imaging, samples fixed with 4% paraformaldehyde (PFA) were further treated with a 2.5% glutaraldehyde aqueous solution at 4 °C for 30 min. Progressive and gradual dehydration steps were carried out rinsing the samples with increasing ethanol solutions (0%, 25%, 50%, 75%, and 100% in deionized water). Samples were successively dried overnight and gold-sputtered before SEM investigation.

2.4. Image Measurements and Statistical Analysis. The measurement of the axonal length and orientation was performed after 5 days of differentiation on the β3-tubulin positive neurites (466 neurites have been evaluated for the PC12 neuron-like cells, 742 for the SH-SY5Y derived neurons) by using the Multi Measure plug-in of ImageJ software (http://rsbweb.nih.gov/ij/). In particular, the neurite orientation was measured as the angle (0−90°) comprised between the neurite and an axis parallel to the ridges. For the flat control substrates, the orientation was assessed with respect to an arbitrary axis. Experiments were carried out in triplicate and data were analyzed with Shapiro normality test, Fligner test for the homogeneity of variances, and Kruskal−Wallis nonparametric test by using *R* software (http://www.r-project.org/). A p-value < 0.05 was considered significant. Orientation angle and neurite length were expressed as median ±95% confidence interval and were shown on box-plots. The neural differentiation efficiency was evaluated by measuring the percentage of the cells immunoreactive for the β3-tubulin neural markers (691 PC12 cells and 1107 SH-SY5Y cells have been evaluated). The cell count was manually performed in triplicate samples by using the Cell Counter plug-in of ImageJ, and data were analyzed using ANOVA, expressed as media ± standard error, and shown on histograms.

2.5. Scanning Ion Conductance Microscopy (SICM) and Force Measurement. The order of magnitude of the forces required to deform a single ridge was roughly estimated by a variant of the scanning ion conductance microscopy, capable to deliver noncontact mechanical stimuli to a sample *via* a glass pipette. In this scanning probe microscopy, the parameter used to control the probe-sample distance is the intensity of the ion current flowing through the pipette aperture. When the pipette approaches a ridge along the X axis, the current decreases because of the reduction of the conducting space. The pipette can be stopped when the ion current (I) is reduced to a preset percentage of its maximum value (I_0), initially measured far from the sample. An external hydrostatic pressure (ΔP) can be applied at the pipette aperture to determine a solution flow. The forces exerted by the flow at the pipette aperture as a function of pipette-sample

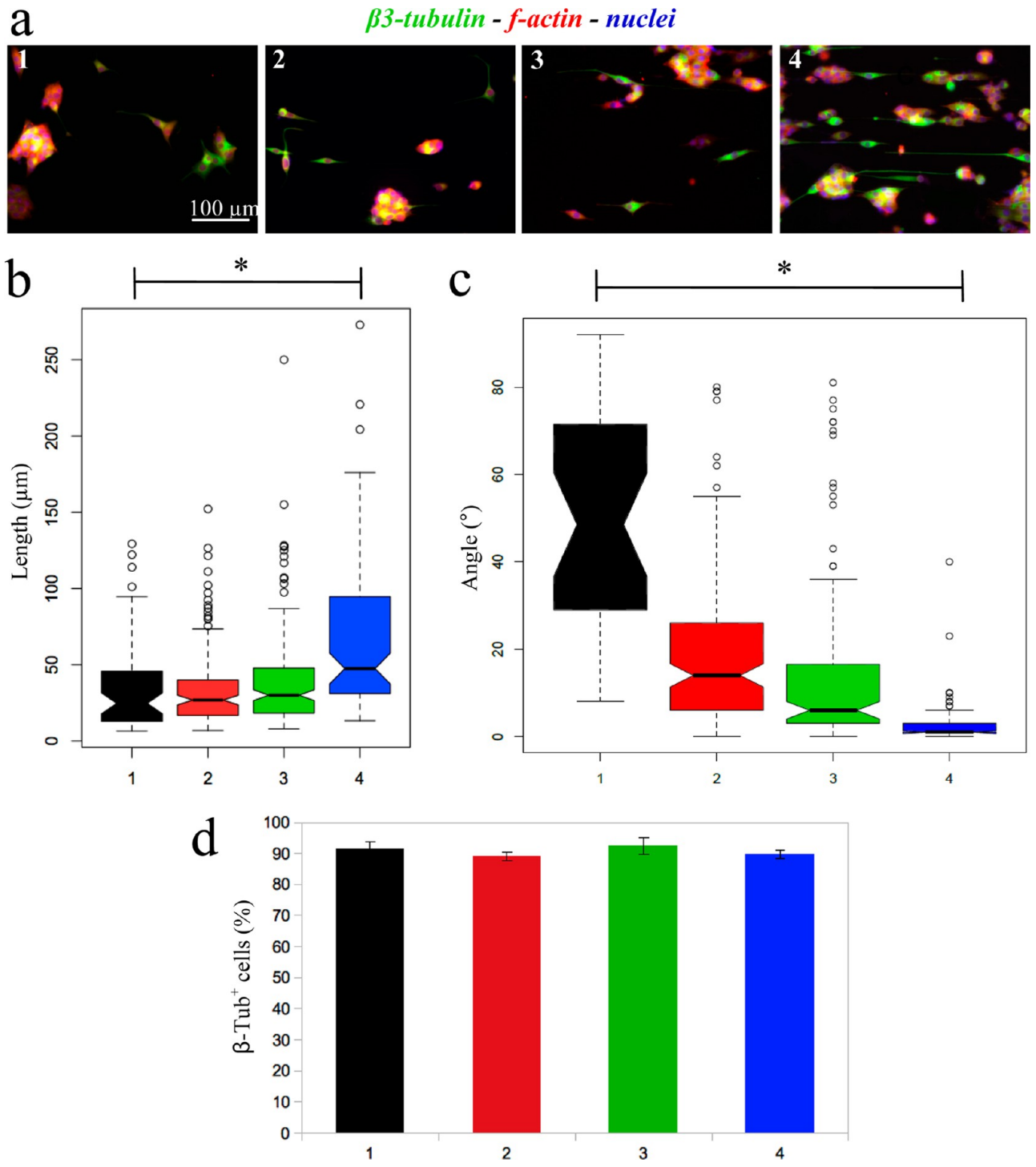

Figure 2. PC12 neuron-like cells differentiated on flat control (substrate 1), and on the patterned surfaces characterized by low, intermediate, and high frequency of ridges (named as substrate 2, 3, 4, respectively). (a) Immunostaining of PC12 cells. In green, β3-tubulin; in red, f-actin; in blue, nuclei. (b) Neurite length distributions of PC12 derived neurons. (c) Neurite orientation distributions of PC12-derived neurons. (d) Histogram of the neuronal differentiation efficiency expressed as the ratio between β3-tubulin-positive cells and total number of cells. * = $p < 0.05$.

distance can thus be derived, as extensively reported in a previous work.[52]

Briefly, assuming the pipette tip orthogonal to the target, the force F acting on the ridge, when the pipette orthogonally approaches the target, changes with the probe-sample distance, being close to its theoretical maximum just before the contact, and it is given by

$$F = \Delta P \pi r^2 \quad (1)$$

where r is the pipette aperture radius.

It has been shown that a pressure ΔP_1 applied to the pipette progressively induces a displacement of the target. Thus, the probe has to approach for an additional distance (δ) to decrease I/I_0 to the same defined preset threshold achieved when $\Delta P = 0$. The target displacement just before the contact (δ_{ct}) can be indirectly obtained by analyzing two I/I_0 vs pipette displacement curves recorded with and without the application of the pressure, in the I/I_0 range between 0.985 and 0.965. δ_{ct} can be calculated by δ, corrected by a factor of 0.46, experimentally determined as described elsewhere.[53]

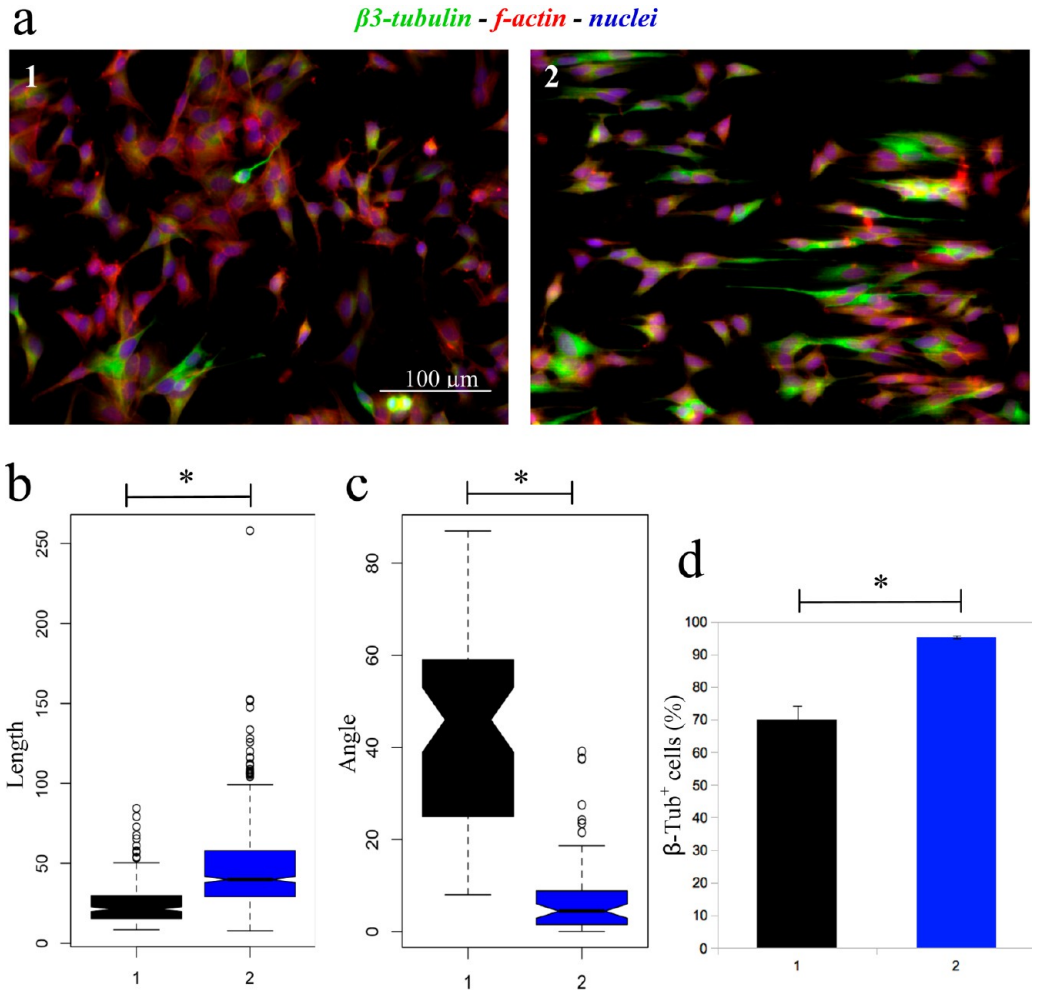

Figure 3. SH SY5Y human neuroblastoma cells differentiated on flat control (substrate 1), and on the patterned surfaces characterized by the highest frequency of aligned ridges (substrate 4). (a) Immunocytochemistry of SH-SY5Y. In green, β3-tubulin; in red, f-actin; in blue, nuclei. (b) Neurite length distributions. (c) Neurite orientation distributions of SH-SY5Y derived neurons. (d) Histogram of the neuronal differentiation efficiency expressed as the ratio between β3-tubulin-positive cells and total number of cells. * = $p < 0.05$.

The pipettes used as probes were made from 1.7/1.1 mm (outer/inner diameter) glass capillaries (7087 Blaubrand, Wertheim, Germany), and had a resistance of 8−18 MΩ. Inner diameter of the tip was between 300 and 500 nm. The pipette, the tip cone angle of which is deviated of about 6° from the pipette main axis, could not be placed parallel to the glass surface and orthogonal to the ridge, the height of which is about 660 nm. In order to approach as close as possible along an orthogonal direction toward the lateral surface of the ridge, a microforge was used to bend by 30° the pipette shaft with respect to its stem. The pipette was subsequently mounted on the piezo-translation stage at 45°, resulting an angle of 75° between the axis of pipette tip and the lateral side of the ridge. The probe was connected to a high-impedance head-stage patch-clamp amplifier (EPC-7) and the bath reference was made by an Ag−AgCl electrode through an agar bridge. The probe was mounted on a piezo translation stage (Nanocube P-611 3S, Physik Instrumente), controlled by a driver (E-664, Physik Instrumente).

Two data acquisition cards (PCI-6251, National Instruments) were used for the DA control of the piezo driver and the AD acquisition of the probe current and piezo sensor signals. The software for both the scan control and data analysis was developed in LabVIEW 8.2.1. The scanning probe microscope was mounted on the stage of an inverted microscope Nikon Diaphot 300, provided with phase-contrast optics.

3. RESULTS

3.1. Submicrometric Patterned Substrate Characterization. In order to guide the axonal outgrowth, we decided to mimic the physical presence of previously aligned axons (the so-called pioneer longitudinal axons)[54] on the glass coverslips where cells have to be cultured. At this purpose, we prepared submicrometric ridges curing the biocompatible Ormocomp resist. In particular, for testing the effects of the ridge spacing frequency on the neuron behavior, we planned to polymerize the submicrometric structures spaced at different distance: 10 μm, 5 μm, and 2.5 μm.

The obtained substrates were characterized by using both AFM and SEM: it is possible to appreciate the different frequencies of regular, aligned, and perfectly polymerized submicrometric structures with both SEM (Figure 1a) and AFM (Figure 1b). SEM high magnification imaging of a single ridge was performed to obtain information about the width of the ridges (Figure 1c), while the high magnification with AFM (Figure 1d) was used to measure the height of the structures.

Furthermore, FIB exposure allowed to mill the ridge and a tilted view with the SEM enabled to show the inner shape and size of the structure (Supporting Information Figure S1). The single ridge resulted about 482 ± 24 nm in width (n = 13) and

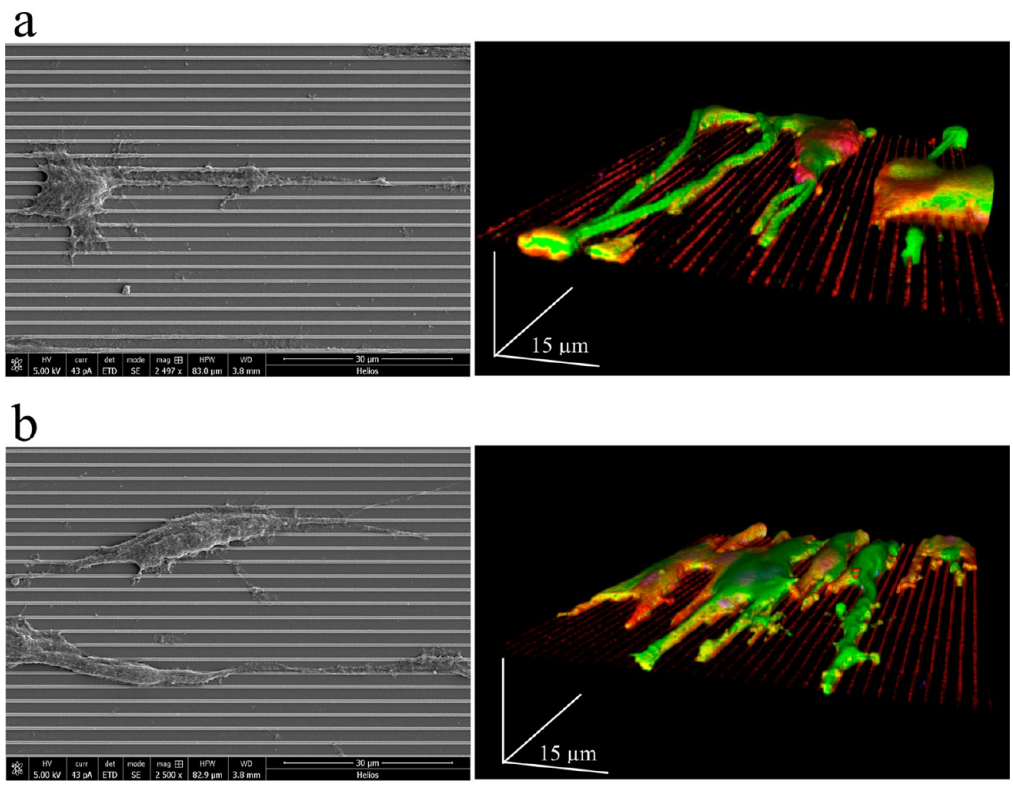

Figure 4. PC12 and SH SY5Y neuron-like cells differentiated on high frequency ridges. SEM images (on the left) and 3D rendering of a *z*-stack confocal acquisition (on the right) of PC12 (a) and SH-SY5Y cells (b).

658 ± 29 nm in height (n = 9), that is, of the same order of magnitude of neurites.[55] No significant differences were detected among the ridges size of the different substrates.

The roughness of the ridges (RMS = 3.20 ± 0.28 nm, n = 9) and of the glass between them (RMS = 1.99 ± 0.19 nm, n = 9) were finally measured, highlighting a significant difference between the two materials (Student's t-test, $p < 0.05$). The roughness values measured on the ridges were consistent with the technical data of the Ormocomp (http://www.microchem.com/PDFs_MRT/Ormocomp%20Overview.pdf). Further details are provided in Supporting Information Figure S2.

3.2. Biological Testing. The PC12 neuron-like cells were differentiated for 5 days on gratings characterized by different frequencies of the ridges, as well as on the flat control substrate (Figure 2a). We observed that, after the differentiation induction, cells grown on the substrates with aligned ridges were characterized by generally longer neurites (26.8 ± 3.1 µm for substrate 2; 30.0 ± 3.5 µm for substrate 3; 47.5 ± 10.2 µm for substrate 4) with respect to the control (24.6 ± 6.9 µm, substrate 1), as reported in details in Figure 2b. In particular, neurite length of PC12 differentiated on the patterned surfaces presenting the highest ridge frequency (substrate 4) was significantly higher compared to the control and to all the other substrates ($p < 0.05$, n = 3).

Alignment of neurites developed on the patterned surfaces was significantly higher (14.0 ± 2.7° for substrate 2; 6.0 ± 2.0° for substrate 3; 1.0 ± 0.3° for substrate 4) with respect to the control (48.5 ± 11.7°, substrate 1, $p < 0.05$, n = 3; Figure 2c). Furthermore, the higher was the frequency of the ridges, the higher was the alignment of the developed neurites, being almost parallel to the ridges on substrate 4.

Collectively, we can affirm that thanks to the submicrometric patterned surfaces prepared through DLW it is possible to guide and promote the axonal outgrowth of the PC12 neuron-like cells. In order to quantify the PC12 differentiation toward neurons, we evaluated the percentage of the cells expressing the peculiar neuronal marker β3-tubulin. After 5 days since the NGF treatment, almost all the cells were immunoreactive for the β3-tubulin in all the considered substrates, and no significant differences among the different groups were found (91.3 ± 2.6% for substrate 1; 89.0 ± 1.3% for substrate 2; 92.4 ± 2.8% for substrate 3, 89.8 ± 1.3% for substrate 4; Figure 2d).

In order to confirm obtained results on other neural models, we differentiated SH-SY5Y human neuroblastoma derived cells for 5 days on the patterned surfaces characterized by the highest frequency of submicrometric structures, which gave the best results in terms of neurite alignment and length, and we analyzed the morphometric properties of the neural branches (Figure 3a). Also, in the case of SH-SY5Y, cells differentiated on the submicrometric patterned surfaces presented a marked neural phenotype, and their neurites resulted to be significantly longer (39.9 ± 2.0 µm) with respect to the flat substrate (21.4 ± 1.5 µm, $p < 0.001$, n = 3; Figure 3b). As previously observed for PC12 cells, the increment in neurite length of the SH-SY5Y neurons differentiated on the aligned ridges is associated with a higher alignment (4.4 ± 1.6°) with respect to the flat control substrate (46.0 ± 7.0°, $p < 0.001$, n = 3; Figure 3c). Furthermore, it was also possible to appreciate a significant increment in the percentage of cells expressing the neuronal marker β3-tubulin (95.3 ± 0.4%) with respect to the control (69.7 ± 3.4%, $p < 0.001$, n = 3; Figure 3d).

All these results demonstrate as the developed submicrometric patterned substrates are able to promote and to improve the neuronal maturation of SH-SY5Y cells, in terms of β3-tubulin expression, neurite length, and neurite orientation.

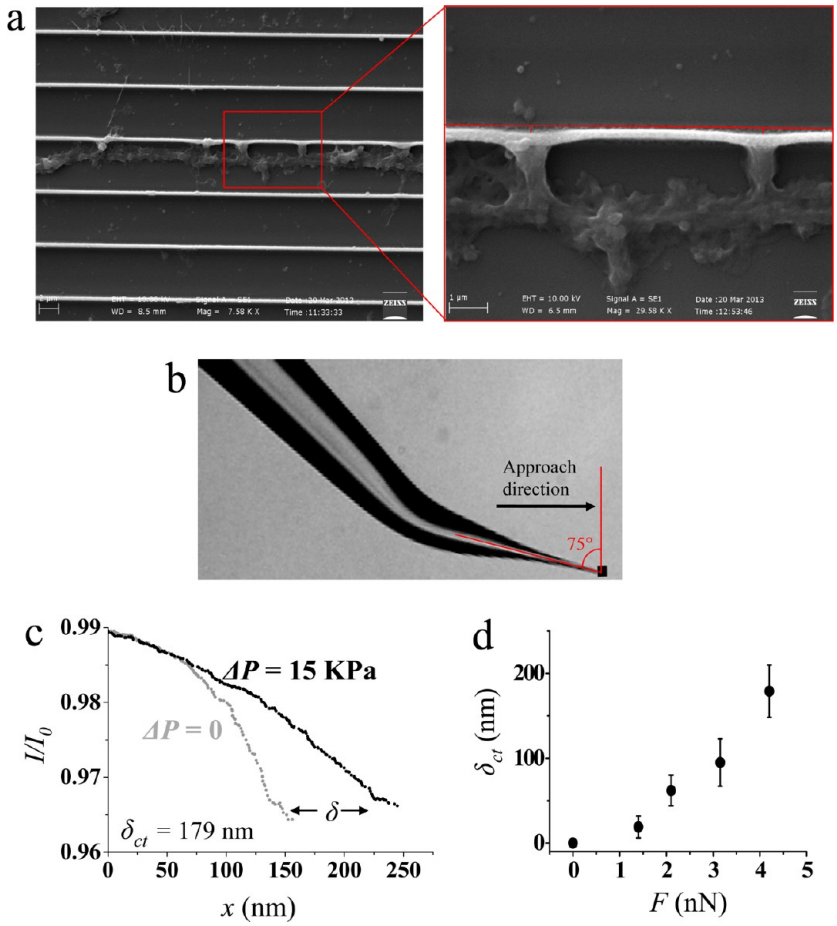

Figure 5. Biomechanical study of the forces applied by a neurite to the submicrometric ridge. (a) SEM image of a PC12 neurite contacting a ridge; the high magnification image shows a neurite pulling the structure at the contact point. (b) Image showing the pipette approaching the target. (c) Two current-displacement curves recorded while a SICM probe approached a ridge: the gray and the black trace were obtained with $\Delta P = 0$ and $\Delta P = 15$ KPa, respectively. The probe was a glass pipette with a tip inner diameter of 500 nm. The ridge displacement (δ_{ct}) was derived by δ in the I/I_0 interval between 0.985 and 0.965, using a correction factor of 0.46. (d) Ridge displacement (δ_{ct}) measured at different values of force (F), with a glass pipette with a tip inner diameter of 300 nm, the points indicate the mean values (±SD) of four measurements.

Finally, thanks to SEM imaging and confocal analysis of the PC12 neuron-like cells (Figure 4a) and of the SH-SY5Y derived neurons (Figure 4b) differentiated on the substrate 4, it has been possible to investigate the 3D environment of the cultures on the gratings. In particular, it is possible to confirm that the sizes of the neural branches are of the same order of magnitude of the topographic submicrometric features photofabricated by DLW. Furthermore, we observed as most of the neurites seem to develop along the space between the aligned ridges, even if there are indeed evidence of some of them growing along or across the ridges. As previously quantitatively observed, the neurites on the patterned surfaces are strongly aligned along the structures.

3.3. Biomechanical Measurements. Patterned substrates can not only mechanically stimulate the cells but, *vice versa*, cells can also produce forces that are able to deform the substrate. We observed that neurons can strongly interact with the submicrometric ridges (Supporting Information Figure S3a), and the vinculin immunocytochemistry analysis showed the formation of well-developed focal adhesions connecting the cell to the submicrometric structures (Supporting Information Figure S3b). Thanks to high magnification SEM imaging, we analyzed the deformations of the ridges at the level of the connection sites produced by the tension developed by PC12 axons. We observed that axon branches were able to contact the ridges, and bend them of about 180 ± 50 nm (Figure 5a). The scheme depicted in Figure 5b shows the noncontact mechanical stimulation carried out by SICM, aimed at inducing a deformation of the ridges similar to those produced by the cells. As already mentioned in the Experimental Section, the SICM pipette could not orthogonally approach the lateral side of the ridges due to the pipette taper. We reached an angle of 75° between the pipette tip and the ridge lateral side, as shown in the Figure 5b; however, this approach did not affect the withdrawn results, as widely demonstrated in Supporting Information (Figure S4).

Figure 5c shows the relation between ion current decrement and pipette displacement toward a ridge, without (gray) and with (black) a pressure $\Delta P = 15$ KPa, corresponding to a force of about 3 nN. This force is necessary to get a target mean displacement just before the contact of 179 nm. Since the axon branches are able to displace a ridge of about 180 nm, and a pipette owing similar size of the cellular protrusions accomplishes an equivalent deformation of the structure by applying a 3 nN force, we can therefore deduce that the cell are applying a force of the same order of magnitude (about 3 nN) at the contact sites with the artificial structures. In order to evaluate the ridge displacements triggered by a wider range of

forces, we also measured the ridge displacement in response to different applied forces, thus obtaining an experimental displacement-force trend, depicted in Figure 5d.

4. DISCUSSION

We have shown for the first time that is possible to promote and guide the axonal outgrowth of two different neural models by using submicrometric topographies photofabricated by Direct Laser Writing. This photolithographic technique allows high-throughput investigations, since it does not require any preliminary process for the preparation of the substrate, such as the fabrication of the masks in photolithographic process, which are heavily time-consuming for the experimenter.

Since past works[46,47] revealed as ridges with sizes comparable to that of the neurites have a remarkable effect on the neurite length and orientation, we decided to mimic the presence of previously aligned axons (the so-called longitudinal pioneer axons) by developing parallel ridges of the biocompatible hybrid polymer Ormocomp. SEM and AFM analyses confirmed the fabrication of regular, parallel structures owing sizes comparable to those of neural branches. In order to test the best conditions in terms of ridge spacing, we prepared three different patterned surfaces characterized by a distance among structures of 10 μm, 5 μm, or 2.5 μm. The axons grown on the latter substrates were strongly aligned and significantly longer compared to the neurites developed on the control flat substrates. These results are in line with other works, where multiple ridges or grooves prepared *via* soft lithography have been used to guide the neurite outgrowth.[43,56] Moreover, the surface roughness analysis revealed a significant difference between the glass and the Ormocomp ridges. Thus, we cannot *a priori* exclude a positive influence of these, even modest, nanofeatures on the neuronal differentiation and on the guidance of the axonal outgrowth.[57]

It is well recognized as surface topographies can not only affect the morphology maturation but also foster cell fate and function. In particular, several investigations suggest that by recreating *in vitro* the features of the *in vivo* extracellular microenvironment of a specific tissue, it is possible to direct the cell differentiation toward a peculiar cell type.[58,59] Concerning the neural differentiation, it has been demonstrated that microtubular structures are able to promote the differentiation of stem cells toward neurons expressing the β3-tubulin,[21] a typical neuronal marker.[60]

In this work, we remarked an increased percentage of β3-tubulin positive SH-SY5Y cells differentiated on the gratings compared to the flat control surfaces, demonstrating that also the molecular differentiation toward the neural phenotype was enhanced thanks to presence of submicrometric features mimicking guiding axons. Concerning the β3-tubulin expression in PC12, we observed a really high expression of this marker on all the substrates. Almost all the cells treated for 5 days with NGF expressed this protein also without the presence of the topographical stimuli. Because of the extremely early expression of β3-tubulin during PC12 differentiation (confirmed by evidence in the literature[61]), it was not possible to detect its modulation on the patterned surfaces; however, their beneficial effects were still demonstrated in terms of neurite length. In SH-SY5Y, on the contrary, β3-tubulin expression is delayed during the differentiation,[62] thus allowing to appreciate an improvement of cell behavior on patterned surfaces even at molecular level.

The surface topographies fabricated by DLW have proven to be not only an interesting tool for the control of the cell morphology and differentiation, but also a high-throughput approach for the study of the mechanobiology of the neurites. Even if the influence of elastic properties of the substrate material on cell behavior is out of the scope of the present paper, we would like to highlight as the Young's modulus of Ormocomp (E = 1.27 GPa)[11] resulted suitable for the investigation of structure deformations produced by the cells. In particular, we demonstrated that it was possible to localize and estimate the force by which the neurites of the cells can deform the substrate. These results are particularly interesting since it is well-known from the literature that the forces exerted and/or sensed by the cells are translated by mechanotransduction phenomena into specific intracellular biochemical pathways, which are involved in tissue remodeling and differentiation.[63] Our data suggest that the axonal branches of PC12 can develop forces of a few nN to deform the ridges. These results are coherent with those obtained on the same material using AFM.[10] Anyhow, we have to stress as the advantage of our approach (by using SICM) with respect to the AFM for this type of measurements is due to the possibility of making straightforward noncontact force measurements.

Forces of the order of a few nN can be sustained by outgrowing neurites of PC12 for several minutes and are essential for the axonal elongation, as shown by Heidemann et al.[64] By measuring the ridge displacements in response to different intensities of interacting forces, we obtained an experimental displacement-force trend. In this way, just by detecting the displacement of a ridge, it is possible to infer the force produced by the cells at the deformed contact point.

The rapid-prototyping and the high reproducibility of these UV-cured structures open new possibilities for further high-throughput investigations, such as the mapping of the forces exerted by the neural culture, as well as the analysis of the mechanotransduction pathways induced by different substrate topographies.

CONCLUSION

This work demonstrates as DLW represents a promising tool for the rapid-prototyping of patterned surfaces, exploitable for the study of physical effects of the substrate features on the cell behavior. In particular, we designed and fabricated aligned submicrometric ridges able to improve the neural differentiation and outgrowth and to control the axonal guidance of different *in vitro* neuronal models.

Furthermore, we were able to detect the displacement of the submicrometric features due to the forces applied by the neurites and thus to infer the order of magnitude of the forces exerted by the axons on the ridges thanks to scanning probe techniques. We therefore successfully exploited DLW for an *in vitro* study of neuron/substrate interactions, demonstrating as this technology can be a promising tool for a wide range of applications, including neuronal tissue engineering, mechanobiology, and biohybrid devices.

Finally, the possibility to photofabricate nanocomposite scaffolds represents an interesting opportunity for conferring new characteristics to the material. Loading the bulk materials with "smart" nanoparticles will have the potential to impart specific properties to the structures (piezoelectric,[30] magnetic,[65] photothermal,[66] *etc.*). This approach, jointly to the possibility of surface functionalization with biologically active molecules,

could become an intriguing platform for the investigation and fostering of cell, and eventually tissue, behaviors.

■ ASSOCIATED CONTENT

Supporting Information

Figure S1: tilted view acquired by SEM of a submicrometric ridge milled by FIB. Figure S2: roughness analysis of the ridge and glass surface. Figure S3: PC12 neuron-like cell adhesion on a submicrometric patterned substrate. Figure S4: control experiments performed for evaluating the pipette positioning effects on the biomechanical measurements. This material is available free of charge via the Internet at http://pubs.acs.org.

■ AUTHOR INFORMATION

Corresponding Author

*E-mail: attilio.marino@iit.it.

Notes

The authors declare no competing financial interest.

■ REFERENCES

(1) Maruo, S.; Nakamura, O.; Kawata, S. *Opt. Lett.* **1997**, *22*, 132−134.
(2) Cumpston, B. H.; Ananthavel, S. P.; Barlow, S.; Dyer, D. L.; Ehrlich, J. E.; Erskine, L. L.; Heikal, A. A.; Kuebler, S. M.; Sandy Lee, I.-Y.; McCord-Maughton, D.; Qin, J.; Rockel, H.; Rumi, M.; Wu, X.-L.; Marder, S. R.; Perry, J. W. *Nature* **1999**, *398*, 51−54.
(3) Malinauskas, M.; Zukauskas, A.; Bickauskaite, G.; Gadonas, R.; Juodkazis, S. *Opt. Express* **2010**, *18*, 10209−10221.
(4) Jeon, H.; Hidai, H.; Hwang, D. J.; Grigoropoulos, C. P. *J. Biomed. Mater. Res. A* **2009**, *2*, 1927−1933.
(5) Claeyssens, F.; Hasan, E. A.; Gaidukeviciute, A.; Achilleos, D. S.; Ranella, A.; Reinhardt, C.; Ovsianikov, A.; Xiao, S.; Fotakis, C.; Vamvakaki, M.; Chichkov, B. N.; Farsari, M. *Langmuir* **2009**, *25*, 3219−3223.
(6) Klein, F.; Richter, B.; Striebel, T.; Franz, C. M.; Freymann, G. V.; Wegener, M.; Bastmeyer, M. *Adv. Mater.* **2011**, *23*, 1341−1345.
(7) Matei, A.; Schou, J.; Canulescu, S.; Zamfirescu, M.; Albu, C.; Mitu, B.; Buruiana, E. C.; Buruiana, T.; Mustaciosu, C.; Petcu, I.; Dinescu, M. *Appl. Surf. Sci.* **2013**, *278*, 357−361.
(8) Culver, J. C.; Hoffmann, J. C.; Poché, R. A.; Slater, J. H.; West, J. L.; Dickinson, M. E. *Adv. Mater.* **2012**, *24*, 2344−2348.
(9) Tayalia, B. P.; Mendonca, C. R.; Baldacchini, T.; Mooney, D. J.; Mazur, E. *Adv. Mater.* **2008**, *20*, 4494−4498.
(10) Klein, F.; Striebel, T.; Fischer, J.; Jiang, Z.; Franz, C. M.; Freymann, G. V.; Wegener, M.; Bastmeyer, M. *Adv. Mater.* **2010**, *22*, 868−871.
(11) Schizas, C.; Karalekas, D. *J. Mech. Behav. Biomed.* **2011**, *4*, 99−106.
(12) Doraiswamy, A.; Jin, C.; Narayan, R. J.; Mageswaran, P.; Mente, P.; Modi, R.; Auyeung, R.; Chrisey, D. B.; Ovsianikov, A.; Chichkov, B. *Acta Biomater.* **2006**, *2*, 267−275.
(13) Ovsianikov, A.; Ostendorf, A.; Chichkov, B. N. *Appl. Surf. Sci.* **2007**, *253*, 6599−6602.
(14) Schilie, S.; Ngezahayo, A.; Ovsianikov, A.; Fabian, T.; Kolb, H. A.; Haferkamp, H.; Chichkov, B. N. *J. Biomater. Appl.* **2007**, *22*, 275−287.
(15) Don Han, E.; Yoon, S.-; Hee Kim, B.; Ho Seo, Y. *Appl. Phys. Lett.* **2013**, *102*, 113701.
(16) Yoon, S. H.; Kim, Y. K.; Han, E. D.; Seo, Y.-H.; Kim, B. H.; Mofrad, M. R. K. *Lab Chip* **2012**, *12*, 2391−2402.
(17) Nikkhah, M.; Edalat, F.; Manoucheri, S.; Khademhosseini, A. *Biomaterials* **2012**, *33*, 5230−5246.
(18) Vogel, V.; Sheetz, M. *Nat. Rev. Mol. Cell. Biol.* **2006**, *7*, 265−275.
(19) Markert, L. D.; Lovmand, J.; Foss, M.; Lauridsen, R. H.; Lovmand, M.; Füchtbauer, E. M.; Füchtbauer, A.; Wertz, K.; Besenbacher, F.; Pedersen, F. S.; Duch, M. *Stem Cells Dev.* **2009**, *18*, 1331−1342.
(20) Fiedler, J.; Ozdemir, B.; Bartholomä, J.; Plettl, A.; Brenner, R. E.; Ziemann, P. *Biomaterials* **2013**, *34*, 8851−8859.
(21) Wang, G.; Ao, Q.; Gong, K.; Wang, A.; Zheng, L.; Gong, Y.; Zhang, X. *Acta Biomater.* **2010**, *6*, 3630−3639.
(22) Ferrari, A.; Cecchini, M.; Degl'Innocenti, R.; Beltram, F. *IEEE Trans. Biomed. Eng.* **2009**, *56*, 2692−2696.
(23) Anene-Nzelu, C. G.; Choudhury, D.; Li, H.; Fraiszudeen, A.; Peh, K. Y.; Toh, Y. C.; Ng, S. H.; Leo, H. L.; Yu, H. *Biomaterials* **2013**, *34*, 5078−5087.
(24) Greco, F.; Fujie, T.; Ricotti, L.; Taccola, S.; Mazzolai, B.; Mattoli, V. *ACS Appl. Mater. Interfaces* **2013**, *5*, 573−584.
(25) Oakley, C.; Jaeger, N. A.; Brunette, D. M. *Exp. Cell. Res.* **1997**, *234*, 413−424.
(26) Bucaro, M. A.; Vasquez, Y.; Hatton, B. D.; Aizenberg, J. *ACS Nano* **2012**, *6*, 6222−6230.
(27) Kolind, K.; Leong, K. W.; Besenbacher, F.; Foss, M. *Biomaterials* **2012**, *336*, 6626−6633.
(28) Genchi, G. G.; Ciofani, G.; Polini, A.; Liakos, I.; Iandolo, D.; Athanassiou, A.; Pisignano, D.; Mattoli, V.; Menciassi, A. *J. Tissue Eng. Regen. Med.* **2012**, DOI: 10.1002/term.1623.
(29) Pellegrino, M.; Orsini, P.; Pellegrini, M.; Baschieri, P.; Dinelli, F.; Petracchi, D.; Tognoni, E.; Ascoli, C. *Neurosci. Res.* **2011**, *69*, 234−240.
(30) Ciofani, G.; Danti, S.; D'Alessandro, D.; Ricotti, L.; Moscato, S.; Bertoni, G.; Falqui, A.; Berrettini, S.; Petrini, M.; Mattoli, V.; Menciassi, A. *ACS Nano* **2010**, *4*, 6267−6277.
(31) Lu, Y. P.; Yang, C. H.; Yeh, J. A.; Ho, F. H.; Ou, Y. C.; Chen, C. H.; Lin, M. Y.; Huang, K. S. *Int. J. Pharm.* **2013**, DOI: 10.1016/j.ijpharm.2013.08.006.
(32) Tsuruma, A.; Tanaka, M.; Yamamoto, S.; Fukushima, N.; Yabu, H.; Shimomura, M. *Colloids Surf., A* **2006**, *284−285*, 470−474.
(33) Weigel, S.; Osterwalder, T.; Tobler, U.; Yao, L.; Wiesli, M.; Lehnert, T.; Pandit, A.; Bruinink, A. *PLoS One* **2012**, *7*, e50714.
(34) Schmidt, C. E.; Leach, J. B. *Annu. Rev. Biomed. Eng.* **2003**, *5*, 293−347.
(35) Marconi, E.; Nieus, T.; Maccione, A.; Valente, P.; Simi, A.; Messa, M.; Dante, S.; Baldelli, P.; Berdondini, L.; Benfenati, F. *PLoS One* **2012**, *7*, e34648.
(36) Dickson, B. J. *Science* **2002**, *298*, 1959−1964.
(37) Moore, S. W.; Sheetz, M. *Dev. Neurobiol.* **2011**, *71*, 1090−10101.
(38) Maskery, S.; Shinbrot, T. *Annu. Rev. Biomed. Eng.* **2005**, *7*, 187−221.
(39) Bak, M.; Fraser, S. E. *Development* **2003**, *130*, 4999−5008.
(40) Miller, C.; Jeftinija, S.; Mallapragada, S. *Tissue Eng.* **2002**, *8*, 367−378.
(41) Koh, H. S.; Yong, T.; Chan, C. K.; Ramakrishna, S. *Biomaterials* **2008**, *29*, 3574−3582.
(42) Micholt, L.; Gärtner, A.; Prodanov, D.; Braeken, D.; Dotti, C. G.; Bartic, C. *PLoS One* **2013**, *8*, e66170.
(43) Johansson, F.; Carlberg, P.; Danielsen, N.; Montelius, L.; Kanje, M. *Biomaterials* **2006**, *27*, 1251−1258.
(44) Ferrari, A.; Faraci, P.; Cecchini, M.; Beltram, F. *Biomaterials* **2010**, *31*, 2565−2573.
(45) Baranes, K.; Kollmar, D.; Chejanovsky, N.; Sharoni, A.; Shefi, O. *J. Mol. Histol* **2012**, *43*, 437−447.
(46) Foley, J. D.; Grunwald, E. W.; Nealey, P. F.; Murphy, C. J. *Biomaterials* **2005**, *26*, 3639−3644.
(47) Fozdar, D. Y.; Lee, J. Y.; Schmidt, C. E.; Chen, S. *Biofabrication* **2010**, *2*, 035005.
(48) Tan, J. L.; Tien, J.; Pirone, D. M.; Gray, D. S.; Bhadriraju, K.; Chen, C. S. *Proc. Natl. Acad. Sci. U.S.A.* **2003**, *100*, 1484−1489.
(49) Balaban, N. Q.; Schwarz, U. S.; Riveline, D.; Goichberg, P.; Tzur, G.; Sabanay, I.; Mahalu, D.; Safran, S.; Bershadsky, A.; Addadi, L.; Geiger, B. *Nat. Cell Biol.* **2001**, *3*, 466−72.
(50) Ganz, A.; Lambert, M.; Saez, A.; Silberzan, P.; Buguin, A.; Mège, R. M.; Ladouxt, B. *Biol. Cell.* **2006**, *8*, 721−730.
(51) Greene, L. A.; Tischler, A. S. *Proc. Natl. Acad. Sci. U.S.A.* **1976**, *73*, 2424−2428.

(52) Hashemi, S. H.; Li, J. Y.; Ahlman, H.; Dahlström, A. *Neurochem. Res.* **2003**, *28*, 449−460.
(53) Pellegrino, M.; Pellegrini, M.; Orsini, P.; Tognoni, E.; Ascoli, C.; Baschieri, P.; Dinelli, F. *Pflugers Arch. Eur. J. Phy.* **2012**, *464*, 307−316.
(54) Farmer, W. T.; Altick, A. L.; Nural, H. F.; Dugan, J. P.; Kidd, T.; Charron, F.; Mastick, G. S. *Development* **2008**, *135*, 3643−3653.
(55) Lee, J. W.; Lee, K. S.; Cho, N.; Ju, B. K.; Lee, K. B.; Lee, S. H. *Actuators B* **2007**, *128*, 252−257.
(56) Jeon, K. J.; Park, S. H.; Shin, J. W.; Kang, Y. G.; Hyun, J.-S.; Oh, M. J.; Kim, S. Y.; Shin, J.-W. *J. Biosci. Bioeng.* 2013, doi: 0.1016/j.jbiosc.2013.08.002, Access Date December 2013.
(57) Bakeine, G. J.; Ban, J.; Grenci, G.; Pozzato, A.; Zilio, S. D.; Prasciolu, M.; Businaro, L.; Tormen, M.; Ruaro, M. E. *Microelectron. Eng.* **2009**, *86*, 1435−1438.
(58) Seo, C. H.; Furukawa, K.; Suzuki, Y.; Kasagi, N.; Ichiki, T.; Ushida, T. *Macromol. Biosci.* **2011**, *11*, 938−945.
(59) Dickinson, L. E.; Kusuma, S.; Gerecht, S. *Macromol. Biosci.* **2011**, *11*, 36−49.
(60) Fabbro, A.; Sucapane, A.; Toma, F. M.; Calura, E.; Rizzetto, L.; Carrieri, C.; Martinelli, V.; Scaini, D.; Masten, L.; Turco, A.; Gustincich, S.; Prato, M.; Ballerini, L. *PLoS One* **2013**, *8*, e73621.
(61) Drubin, D. G.; Feinstein, S. C.; Shooter, E. M.; Kirschner, M. W. *J. Cell. Biol.* **1985**, *101*, 1799−1807.
(62) Hau, S.; Reich, D. M.; Scholz, M.; Naumann, W.; Emmrich, F.; Kamprad, M.; Boltze, J. *BMC Neurosci.* **2008**, *9*, 30.
(63) Fu, J.; Wang, Y. K.; Yang, M. T.; Desai, R. A.; Yu, X.; Liu, Z.; Chen, C. S. *Nat. Methods* **2010**, *7*, 733−736.
(64) Heidemann, S. R.; Lamoureux, P.; Buxbaum, R. E. *Cell. Biochem. Biophys.* **1995**, *27*, 135−155.
(65) Taccola, S.; Greco, F.; Zucca, A.; Innocenti, C.; De Julián Fernández, C.; Campo, G.; Mattoli, V. *ACS Appl. Mater. Interfaces* **2013**, *5*, 6324−6332.
(66) FarrokhTakin, E.; Ciofani, G.; Gemmi, M.; Piazza, V.; Mazzolai, B.; Mattoli, V. *Colloids Surf., A* **2012**, *415*, 247−254.